

FlashLips: 100-FPS Mask-Free Latent Lip-Sync using Reconstruction Instead of Diffusion or GANs

Andreas Zinonos^{1*} Michał Stypułkowski² Antoni Bigata¹
 Stavros Petridis^{1,3} Maja Pantic^{1,3} Nikita Drobyshev^{2*}
¹Imperial College London ²Cantina Labs ³NatWest

{andreas.zinonos18, a.bigata-casademunt22, stavros.petridis04, m.pantic}@imperial.ac.uk
 {nikita, michal.stypulkowski}@cantina.ai



Figure 1. **FlashLips Results.** Selected results of source and driver pairs, generated using our transformer-based model.

Abstract

We present FlashLips, a two-stage, mask-free lip-sync system that decouples lips control from rendering and achieves real-time performance running at over 100 FPS on a single GPU, while matching the visual quality of larger state-of-the-art models. Stage 1 is a compact, one-step latent-space editor that reconstructs an image using a reference identity, a masked target frame, and a low-dimensional lips-pose vector, trained purely with reconstruction losses – no

GANs or diffusion. To remove explicit masks at inference, we use self-supervision: we generate mouth-altered variants of the target image, that serve as pseudo ground truth for fine-tuning, teaching the network to localize edits to the lips while preserving the rest. Stage 2 is an audio-to-pose transformer trained with a flow-matching objective to predict lips-poses vectors from speech. Together, these stages form a simple and stable pipeline that combines deterministic reconstruction with robust audio control, delivering high perceptual quality and faster-than-real-time speed.

*Equal Contribution

1. Introduction

Lip synchronization (lip-sync) is the task of regenerating realistic mouth movements that match audio while preserving identity, expression, head pose, background, and overall fidelity of a talking-person video. It has a transformative impact across domains — from automating film/TV dubbing and breaking language barriers, to creating expressive animations and lifelike digital avatars [62, 63]. The central challenge is synthesizing photorealistic, temporally stable lip motions precisely synchronized with speech.

Audio-driven facial generation is closely related: it animates the full face from a reference image and a driving audio [6, 47, 48, 53, 65]. Compared to full-face generation, lip-sync is more controllable and efficient: it edits only the mouth while reusing identity, pose, and background from the target video, crucial for dubbing/localization.

The pursuit of high fidelity has produced a spectrum of deep learning approaches [11]. Early successes were driven by GANs [12, 13, 35], which can yield sharp frames but are notoriously difficult to train and sensitive to hyperparameters [37, 41]. More recently, iterative generative models — particularly diffusion — have set a strong bar for visual quality in both general face animation [10, 40, 42, 59] and task-specific lip-sync [4, 28, 32]. However, diffusion requires sequential inference (multiple denoising steps), compounding cost and often prompting additional pre/post-processing such as explicit mouth masks or alignment to canonical templates [2, 26], which complicates real-time deployment and adds engineering overhead.

In this work, we take a step back and question the necessity of iterative *visual* generators for a highly conditioned task like lip-sync. We argue that with sufficient context — a reference identity, a target frame, and precise lips-pose cues — a powerful *deterministic* image update can be learned without adversarial objectives or diffusion schedules.

We introduce a lightweight, two-stage framework that separates *control* from *rendering* in the spirit of two-stage designs of [28].

Stage 1: Latent Visual Editor. We start with a compact *one-step* editor operating in VAE latent space [34]. Given a reference image, a target frame, and a low-dimensional *lips-pose vector*, it reconstructs the edited frame in a single feed-forward pass using *reconstruction losses only* - no adversarial training or diffusion.

Our final editor runs *without* explicit mouth masks at inference. After reconstruction training, we self-refine by synthesizing mouth-altered variants and fine-tuning on symmetric *source* \leftrightarrow *changed* pairs, which focuses edits on the lips while preserving the rest of the frame without any external segmentation. Prior work established mask-free feasibility [33]; we instead create the supervision *on-the-fly* with the editor itself, avoiding dataset-constructed pseudo-pairs.

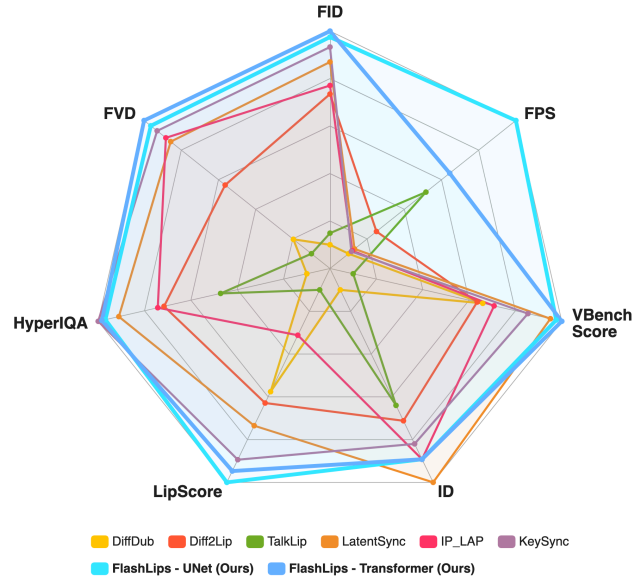


Figure 2. **Visualization of Quantitative Evaluation.** Comparison of eight different lip-sync models in the cross-audio setting on seven key metrics. All results are normalized, with the best-performing model scaled to the outer edge, and the worst scaled towards the center.

Stage 2: Audio-to-Lips. *Stage 2* connects audio to the visual editor via an audio-to-lips transformer that predicts lips-pose vectors from speech. A key design principle is to *disentangle* the control space so that it carries *pose* information only, *i.e.* what the lips should do, while appearance (teeth, lip color, skin tone, jawline) and scene details are sourced from the reference and target frames in Stage 1. This mirrors what can be reliably inferred from audio and keeps Stage 2 lightweight and stable to train. Overloading audio with appearance factors makes learning harder and harms generalization; our disentangled control avoids this by construction. Conditioning on wav2vec 2.0 features [1] and training with *flow-matching* [27, 29] yields smooth control latents that drive the editor.

Our contributions:

- **Real-time performance:** >100 FPS on a single NVIDIA H100 80GB HBM3 that matches or exceeds larger, slower baselines in terms of lip-sync accuracy and quality (Fig. 2).
- **Deterministic, one-step feasibility:** For a highly conditioned task (such as lip-sync), reconstruction-only training might be sufficient, removing the need for adversarial or iterative generators — *no GANs or diffusion*.
- **Mask-free self-refinement:** no explicit mouth masks at inference; fewer mouth artifacts and a simpler pipeline.
- **Disentangled audio-to-pose:** flow-matching transformer on wav2vec 2.0 separates *what* to render from *how* to render, supporting modular, per-component control.

2. Related Work

2.1. Audio-driven Portrait Animation

Audio-driven portrait animation synthesizes talking-head videos from speech [18, 19, 44], yet its objectives differ fundamentally from lip synchronization. It follows an image-to-video paradigm that freely modifies head pose and facial expressions without constraining the output to match a specific input video. In contrast, lip synchronization operates in a video-to-video setting, modifying only the mouth region while preserving all other facial details, effectively editing the original video.

Early GAN-based approaches employed temporal and task-specific discriminators to animate faces [46, 47, 65], later incorporating head-pose modeling to improve the results, though often introducing visual artifacts [58, 66]. Diffusion-based methods further enhanced temporal coherence and perceptual quality [19, 42, 53], sometimes leveraging facial landmarks or 3D meshes [52, 56], although the latter can lead to unrealistic animations. Frameworks with a two stage inference [3] first generate intermediate keyframes and then interpolate between them to achieve smoother, temporally consistent motion. Despite producing plausible facial motion, many of these models suffer from high inference latency. To address this, recent works [23, 54] train small audio-to-latent diffusion models that drive pre-trained latent-to-video decoders, achieving near real-time performance.

Although these methods have advanced portrait animation, their freedom to alter head pose and expression makes them unsuitable for lip synchronization, motivating dedicated methods that preserve identity and facial consistency.

2.2. Audio-driven Lip Synchronization

Lip synchronization aims to modify only the mouth region to match the input audio while preserving head pose, identity, and other facial expressions. Wav2Lip [35] popularized SyncNet-based [7] supervision to ensure reliable audio-visual alignment. Subsequent works such as DINet [62], IP-LAP [64], and ReSyncer [14] enhance realism through spatial deformation of reference features, intermediate landmark prediction, or the use of 3D priors. Other works such as StyleSync [13] and StyleLipSync [22] adopt StyleGAN-inspired architectures [21], while TalkLip [49] leverages a lip-reading expert within a contrastive learning framework to enhance lip-speech synchronization.

Diffusion-based approaches further enhance temporal consistency and perceptual quality [4, 28, 32, 33]. Latent diffusion frameworks such as LatentSync [26] and SayAnything [31] synthesize lip-synced frames directly from audio without intermediate motion conditioning. MuseTalk [60] refines synchronization by selecting reference frames with similar head poses, and KeySync [2] mitigates temporal in-

consistency and leakage through a keyframe-interpolation approach and careful masking strategy.

Nevertheless, existing approaches still face notable limitations. GAN-based methods often suffer from visual artifacts and unstable training, while diffusion-based models, although capable of high-quality synthesis, remain computationally expensive and generally too slow for real-time inference. Moreover, many pipelines depend on extensive pre-processing (e.g., face alignment or intermediate motion estimation), which can introduce artifacts and reduce flexibility. These challenges motivate our work: a simple and efficient framework for high-quality lip synchronization that eliminates iterative generation and heavy pre-processing, enabling faster-than-real-time inference with high-resolution outputs.

3. Method

We propose a two-stage framework for lip synchronization (Fig. 3). **Stage 1** is a fast, deterministic editor that produces high-quality lip-synced frames in a single forward pass. **Stage 2** is an audio-to-pose transformer that predicts low-dimensional lip poses from speech and drives Stage 1. Stage 1 is trained *only* with reconstruction objectives (no adversarial training or diffusion); Stage 2 uses a flow-matching objective.

3.1. Stage 1: Latent Visual Editor

3.1.1. Reconstruction and Lips Encoder

Stage 1 is trained per frame in latent space following [36]. Let $\mathbf{x}_{\text{src}}, \mathbf{x}_{\text{ref}} \in \mathbb{R}^{C \times H \times W}$ be the frame to edit (“source”) and a reference frame from the same video, sampled t frames apart, respectively. During reconstruction training we apply a mouth-region mask to \mathbf{x}_{src} , yielding $\mathbf{x}_{\text{masked}}$.

We encode $\mathbf{x}_{\text{src}}, \mathbf{x}_{\text{masked}}$, and \mathbf{x}_{ref} with the SDXL VAE [24, 34] to obtain latents $\mathbf{z}_{\text{src}}, \mathbf{z}_{\text{masked}}, \mathbf{z}_{\text{ref}} \in \mathbb{R}^{C_\ell \times H_\ell \times W_\ell}$. A small trainable *reference* backbone f_{ref} projects the reference latent, $\bar{\mathbf{z}}_{\text{ref}} = f_{\text{ref}}(\mathbf{z}_{\text{ref}})$, so the model can better adapt identity features. We also use a lips-pose representation $\mathbf{z}_{\text{lips}} \in \mathbb{R}^M$ that encodes lips configuration. It is expanded spatially by replication, $\mathbf{z}_{\text{lips expanded}} \in \mathbb{R}^{M \times H_\ell \times W_\ell}$.

The network’s input is the channel-wise concatenation:

$$\mathbf{z}_{\text{input}} = \text{Concat} [\mathbf{z}_{\text{masked}}, \bar{\mathbf{z}}_{\text{ref}}, \mathbf{z}_{\text{lips expanded}}]. \quad (1)$$

It predicts a latent residual towards the ground-truth edit. With:

$$\mathbf{z}_{\text{target}} = \mathbf{z}_{\text{src}} - \mathbf{z}_{\text{masked}}, \quad (2)$$

the model outputs $\hat{\mathbf{z}}_{\text{target}}$ and forms:

$$\hat{\mathbf{z}}_{\text{src}} = \mathbf{z}_{\text{masked}} + \hat{\mathbf{z}}_{\text{target}}. \quad (3)$$

Decoding with the frozen VAE yields $\hat{\mathbf{x}}_{\text{src}} = \text{VAE}_{\text{decoder}}(\hat{\mathbf{z}}_{\text{src}})$.

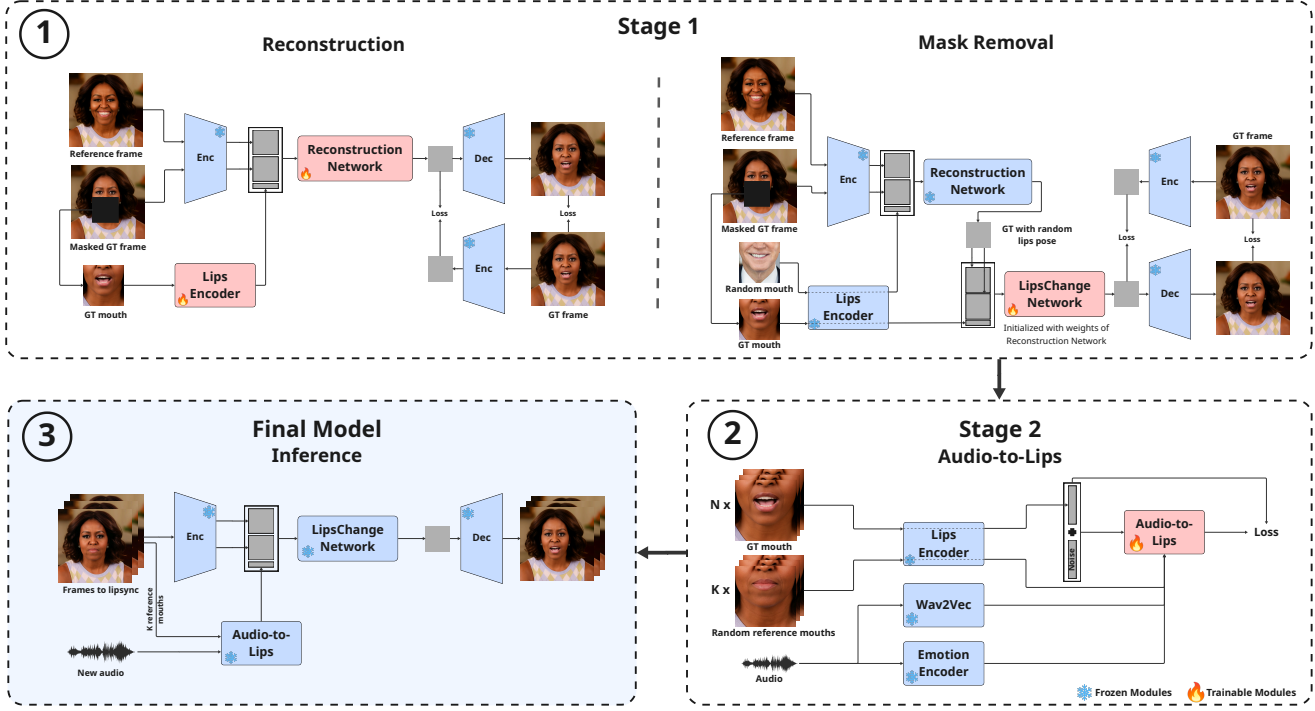


Figure 3. **Overview of FlashLips.** **Stage 1** trains a one-step latent-space editor: first via masked reconstruction, then via a mask-free self-refinement step that learns to localize edits without segmentation. **Stage 2** trains an audio-to-lips model that predicts the lips-pose vector used in Stage 1. At inference, predicted lip poses drive the LipsChange network to produce lip-synced frames in a single pass.

Lips-Pose Representation. We design the representation to carry *only* lip/jaw configuration to predict it more easily from audio. A frozen expression encoder [9] with a small MLP yields $\mathbf{z}_{\text{lips}}^{\text{main}} \in \mathbb{R}^M$. In parallel, a lightweight CNN on a mouth crop predicts a small residual $\mathbf{z}_{\text{lips}}^{\text{add}}$. The final control is $\mathbf{z}_{\text{lips}} = \mathbf{z}_{\text{lips}}^{\text{main}} + \mathbf{z}_{\text{lips}}^{\text{add}}$. For faster inference, we distill these two models into a compact image encoder (e.g., a ResNet-34 head [15]) that predicts \mathbf{z}_{lips} directly from an RGB face crop; see Fig. 4 and the supplementary. Stage 2 is trained to predict the same vector from audio.

3.1.2. Mask Removal via Self-Refinement

Once the reconstruction model converges, we sample lips vectors and synthesize lip-altered variants of the original frames to create symmetric pseudo-pairs (source \rightarrow changed) and (changed \rightarrow source). A *LipsChange* network initialized from the reconstruction model weights is then fine-tuned on these pseudo-pairs. This teaches the model to localize edits to the lips and preserve surrounding regions, eliminating the need for external segmentation (Fig. 3).

3.1.3. Losses

Let \mathbf{M} be the lower-face pixel mask, and \mathbf{m} its latent version downsampled with VAE. Lips mask \mathbf{M}_{lips} comes from face parsing.

Let $\text{MAE}_{\mathbf{w}}(A) = \frac{1}{|\Omega_{\mathbf{w}}|} \|\mathbf{w} \odot A\|_1$ and $\text{MAE}(A) =$

$\frac{1}{|\Omega|} \|A\|_1$, where $\Omega_{\mathbf{w}}$ indicates a support after applying the mask \mathbf{w} , and \odot is the element-wise (Hadamard) product.

Let $\Delta \mathbf{z} = \hat{\mathbf{z}}_{\text{target}} - \mathbf{z}_{\text{target}}$ be the difference between predicted and ground-truth latents. Then, the losses in the latent space are defined as:

$$\mathcal{L}_{L1}^{\text{lat}} = \text{MAE}(\Delta \mathbf{z}), \quad \mathcal{L}_{L1m}^{\text{lat}} = \text{MAE}_{\mathbf{m}}(\Delta \mathbf{z}). \quad (4)$$

We also use the following losses in the pixel space:

$$\mathcal{L}_{L1M}^{\text{pix}} = \text{MAE}_{\mathbf{M}}(\hat{\mathbf{x}}_{\text{src}} - \mathbf{x}_{\text{src}}), \quad (5)$$

$$\mathcal{L}_{L1\text{lips}}^{\text{pix}} = \mathbb{1}_{\{|\Omega_{\text{lips}}| \geq \tau_{\text{lips}}\}} \text{MAE}_{\mathbf{M}_{\text{lips}}}(\hat{\mathbf{x}}_{\text{src}} - \mathbf{x}_{\text{src}}), \quad (6)$$

$$\mathcal{L}_{VGG} = \sum_l \text{MAE}(\phi_l(\hat{\mathbf{x}}_{\text{src}}) - \phi_l(\mathbf{x}_{\text{src}})), \quad (7)$$

$$\mathcal{L}_{VGG}^{\text{face}} = \sum_l \text{MAE}(\psi_l(\hat{\mathbf{x}}_{\text{src}}) - \psi_l(\mathbf{x}_{\text{src}})), \quad (8)$$

where $\hat{\mathbf{x}}_{\text{src}}$ and \mathbf{x}_{src} are predicted and ground-truth images, respectively, \mathcal{L}_{VGG} uses VGG-19 features as in [20], and $\mathcal{L}_{VGG}^{\text{face}}$ uses a VGGFace2-pretrained network [5]. The lips loss is applied only when a valid lips mask is found and its area exceeds τ_{lips} .

Finally, the total loss becomes:

$$\mathcal{L}_{\text{total}} = 0.1 \mathcal{L}_{L1}^{\text{lat}} + 0.1 \mathcal{L}_{L1m}^{\text{lat}} + 10 \mathcal{L}_{L1M}^{\text{pix}} + 100 \mathcal{L}_{L1\text{lips}}^{\text{pix}} + 50 \mathcal{L}_{VGG} + 5 \mathcal{L}_{VGG}^{\text{face}}. \quad (9)$$

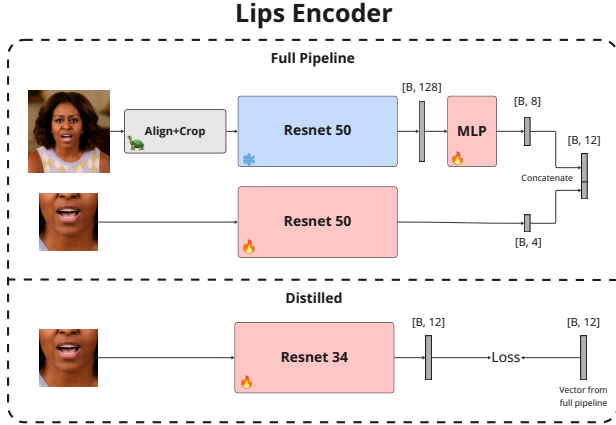


Figure 4. **Lips Encoder.** A frozen expression encoder with an MLP projector and a mouth-crop CNN produce an 8D+4D lips vector. A distilled ResNet-34 replicates this mapping on inference.

3.2. Stage 2: Audio-to-Lips with Flow Matching

Stage 2 predicts the lips vector from speech and drives the editor trained in Stage 1. The model is a transformer conditioned on wav2vec 2.0 features [1]. We train it with a flow-matching objective [27, 29] in the space of lips vectors.

Let \mathbf{a} be the audio features aligned to a video frame, and $\mathbf{z}_{\text{mouth}}$ the target lips vector. We follow the optimal transport conditional flow-matching. We sample $\epsilon \sim \mathcal{N}(0, \mathbf{I})$ and $t \sim \mathcal{U}(0, 1)$, and define an interpolated point in latent space

$$\mathbf{z}_t = (1 - t) \epsilon + t \mathbf{z}_{\text{lips}}, \quad (10)$$

and the target velocity

$$\mathbf{u} = \mathbf{z}_{\text{lips}} - \epsilon. \quad (11)$$

The transformer v_θ is trained to match this velocity field,

$$\mathcal{L}_{\text{FM}} = \mathbb{E}_{t, \epsilon, \mathbf{a}} \|\mathbf{v}_\theta(\mathbf{z}_t, t, \mathbf{c}) - \mathbf{u}\|_2^2, \quad (12)$$

where $\mathbf{c} = \text{Concat}[\mathbf{a}, e(\mathbf{a}), \mathbf{z}_{\text{lips}}^K]$, $e(\mathbf{a})$ is a pre-trained audio emotion encoder, and $\mathbf{z}_{\text{lips}}^K$ are K randomly sampled source lip latents.

At inference, we predict the lips pose $\hat{\mathbf{z}}_{\text{lips}}$ from audio and source lip latents, then pass it to Stage 1.

4. Experiments

We evaluate *FlashLips* end-to-end under two standard protocols: (i) *reconstruction* (same-clip audio) and (ii) *cross-audio* (driven by a different clip). For both settings, we report lip-audio synchronization, visual quality, identity preservation, and runtime efficiency. The full set of metrics is defined in Sec. 4.3. Unless noted otherwise, implementation details (model sizes, preprocessing, schedules) are in the supplementary.

4.1. Datasets

A key advantage of our design is that training the most compute-heavy component (Stage 1) does *not* require audio or even lip-sync supervision: we only need images with a visible mouth. This allows us to leverage substantially broader data than typical lip-sync pipelines.

Stage 1 (image-only). We train the reconstruction/self-refinement editor on MEAD [50], FEED [9], HDTF [61], NeRSemble [25], CelebV-Text [55], CelebV-HQ [67], and a private collection of controlled laboratory recordings with diverse facial expressions (~ 500 hours).

Stage 2 (audio-visual). For audio-to-lips, we use Hallo3 [8], RAVDESS [30], MEAD, HDTF, NeRSemble, CelebV-Text, CelebV-HQ, and our private dataset. Stage 2 is trained to predict the lips vector from speech features.

For quantitative evaluation, we randomly sample 100 reconstruction videos and 100 cross-audio pairs from HDTF, CelebV-HQ and CelebV-Text eval sets.

4.2. Training Details

Stage 1 (Reconstruction & LipsChange). For the one-step editor, we have two backbone versions: a UNet with 250M parameters and a ViT-like visual transformer with 300M. Both are optimized with AdamW and a OneCycleLR schedule: the learning rate starts at 1×10^{-4} and anneals to 1×10^{-8} . We train the reconstruction phase for 1 million iterations on $8 \times$ NVIDIA H100 80GB HBM3 GPUs with a total batch size of 32. After convergence, we train the mask-free self-refinement *LipsChange* (Sec. 3.1.2) using symmetric *source* \leftrightarrow *changed* pseudo-pairs for 200k iterations.

Lips Encoder and distillation. As shown in Fig. 4, our *Lips Encoder* starts from a frozen expression encoder [9] that maps a face crop to an expression latent, followed by a small trainable head (ResNet-50 + MLP) that projects to the compact lips-pose vector used by Stage 1. We train this head during the Stage 1 reconstruction phase. To remove pre-processing overhead at inference (the expression backbone requires several alignment/cropping steps), we *distill* the pipeline into a single ResNet-50 that consumes the full image and predicts the same lips-pose vector. Distillation is performed by matching the outputs of the full pipeline over the last 200k iterations of Stage 1 reconstruction training.

Stage 2 (Audio-to-Lips). Stage 2 is a transformer conditioned on wav2vec 2.0 features, emotion class inferred from audio, and K random lip latents and trained with a conditional flow-matching objective in the lips-pose vector space (Sec. 3.2). We use the same lips-pose vector definition as Stage 1 to ensure compatibility. For training, we utilize the AdamW optimizer with default parameters and a constant 5×10^{-5} learning rate. The transformer backbone has 150M parameters. Additional architectural details are provided in the supplementary.

Model	FID ↓	FVD ↓	HyperIQA ↑	VBench ↑	LipScore ↑	ID ↑	PSNR ↑	SSIM ↑	LPIPS ↓
Reconstruction									
DiffDub [28]	16.11	120.24	57.91	0.673	0.37	0.58	26.65	0.89	0.114
Diff2Lip [32]	8.76	57.96	68.31	0.672	0.47	0.79	25.64	0.94	0.056
TalkLip [49]	13.97	78.66	64.52	0.667	0.57	0.79	32.03	0.94	0.062
LatentSync [26]	5.30	36.47	73.10	<u>0.682</u>	0.55	0.86	33.61	0.97	0.015
IP-LAP [64]	7.91	39.89	69.57	0.674	0.40	0.82	<u>32.97</u>	<u>0.95</u>	0.033
KeySync [2]	5.48	24.80	74.18	0.681	0.56	0.81	30.39	0.93	0.030
FlashLips – UNet (Ours)	<u>4.75</u>	<u>15.20</u>	73.81	0.687	<u>0.70</u>	<u>0.85</u>	32.86	0.94	0.022
FlashLips – Transformer (Ours)	4.43	12.31	<u>74.06</u>	0.687	0.71	0.86	32.88	0.94	<u>0.021</u>
Cross-Audio									
DiffDub [28]	18.31	123.34	57.91	0.668	0.30	0.59	–	–	–
Diff2Lip [32]	9.55	80.43	69.01	0.667	0.31	0.76	–	–	–
TalkLip [49]	17.64	134.70	64.62	0.645	0.21	0.74	–	–	–
LatentSync [26]	7.69	46.08	72.52	0.680	0.33	0.84	–	–	–
IP-LAP [64]	9.05	43.13	69.49	0.670	0.25	<u>0.81</u>	–	–	–
KeySync [2]	6.81	37.55	74.13	0.676	0.36	0.79	–	–	–
FlashLips – UNet (Ours)	<u>6.23</u>	<u>33.57</u>	73.58	<u>0.681</u>	0.38	<u>0.81</u>	–	–	–
FlashLips – Transformer (Ours)	5.89	29.40	<u>73.84</u>	0.682	<u>0.37</u>	<u>0.81</u>	–	–	–

Table 1. **Quantitative Comparison.** Comparison on reconstruction and cross-audio scenarios over 100 randomly sampled reconstruction videos and 100 cross-audio pairs from HDTF, CelebV-HQ, and CelebV-Text. Best results are **bold**; second-best are underlined.

Model	FPS ↑	Speedup ×
DiffDub [28]	1.86	58.8
Diff2Lip [32]	19.77	5.5
TalkLip [49]	51.53	2.1
LatentSync [26]	5.70	19.2
IP-LAP [64]	4.24	25.8
KeySync [2]	3.60	30.4
FlashLips – UNet (Ours)	109.41	1.0
FlashLips – Transformer (Ours)	<u>66.84</u>	1.6

Table 2. **Inference Speed.** Speed comparison in frames per second (FPS). “Speedup” denotes the inference speed gain of our fastest model (FlashLips – UNet) over each method. Measured on the same clip: 5 warm-ups, then 10 runs to average FPS.

4.3. Evaluation Metrics

We evaluate models using a diverse set of metrics that target lip–audio synchronization, visual quality, identity preservation, and efficiency.

To assess lip–audio synchronization accuracy, we use LipScore [3]. For reconstruction fidelity and perceptual quality, we adopt both reference-based and no-reference metrics: Fréchet Inception Distance (FID) [16] at the frame level and Fréchet Video Distance (FVD) [45] at the video level for overall visual quality and temporal consistency; LPIPS [57] as a reference-based perceptual similarity measure; and HyperIQA [43] as a no-reference image-quality metric correlated with human perception. We also report Peak Signal-to-Noise Ratio (PSNR) and Structural Similar-

# Ref. Lats	FVD ↓	HyperIQA ↑	LipScore ↑	ID ↑	PSNR ↑
Reconstruction					
1	12.53	74.05	0.69	<u>0.85</u>	32.71
4	12.31	74.06	0.71	0.86	32.88
8	12.47	<u>74.07</u>	0.73	<u>0.85</u>	33.00
16	11.90	74.08	0.74	0.86	33.02
32	<u>12.16</u>	74.08	0.75	0.86	33.10
Cross-Audio					
1	41.38	73.80	0.40	0.79	–
4	29.40	73.84	<u>0.37</u>	<u>0.81</u>	–
8	29.54	73.88	0.35	<u>0.81</u>	–
16	<u>26.35</u>	<u>73.88</u>	0.34	<u>0.81</u>	–
32	25.16	73.89	0.32	0.82	–

Table 3. **Reference Latent Ablation (Transformer).** Ablation of the number of reference latents for the Transformer base model on a subset of metrics. Full ablations are in Table C.5.

ity Index (SSIM) [51] for pixel-level structural similarity.

To evaluate identity preservation, we define an identity (ID) metric as the cosine similarity between predicted and ground-truth face embeddings computed per frame using FaceNet-512 [38, 39]. For overall visual consistency, we report VBench [17] scores: Subject Consistency (SC), Background Consistency (BC), Motion Smoothness (MS), Dynamic Degree (DD), Aesthetic Quality (AQ), Imaging Quality (IQ), and an aggregated “Total” - the mean of the normalized metrics.

Finally, to measure efficiency, we report inference speed in frames per second (FPS). For each model, the same clip is processed 5 times for warm-up and 10 times for measurement, and we report the average runtime over the measured runs.

# Ref. Lats	FVD ↓	HyperIQA ↑	LipScore ↑	ID ↑	PSNR ↑
Reconstruction					
1	15.68	73.79	0.67	0.85	32.74
4	<u>15.20</u>	73.81	<u>0.70</u>	0.85	32.86
8	15.61	<u>73.82</u>	<u>0.70</u>	0.85	32.92
16	15.07	73.83	0.71	0.85	<u>32.95</u>
32	15.85	73.83	0.69	0.85	32.97
Cross-Audio					
1	42.78	73.51	0.40	0.79	–
4	33.57	73.58	<u>0.38</u>	0.81	–
8	32.64	<u>73.61</u>	0.36	<u>0.80</u>	–
16	<u>31.34</u>	73.63	0.34	0.81	–
32	28.54	73.63	0.32	0.81	–

Table 4. **Reference Latent Ablation (UNet)**. Ablation of the number of reference latents for the UNet base model on a subset of metrics. Full ablations are provided in Table C.5.

Lips Encoder Variant	PSNR ↑	SSIM ↑	LipScore ↑	ID ↑
	Reconstruction		Cross-Audio	
V1 2D	27.11	0.88	0.30	0.83
V1 4D	30.74	0.91	0.32	0.83
V1 8D	31.63	0.93	0.34	0.83
V1 16D	31.95	0.93	0.34	<u>0.82</u>
V1 8D + V2 2D	32.16	0.93	0.36	0.81
V1 8D + V2 4D	32.86	0.94	<u>0.38</u>	0.80
V1 8D + V2 8D	<u>34.86</u>	<u>0.95</u>	<u>0.38</u>	0.74
V1 8D + V2 16D	36.86	0.97	0.40	0.63

Table 5. **Lips Encoder Ablation**. V1 (frozen expression encoder) saturates near 8D; adding a lips-crop residual (V2) improves reconstruction but reduces cross-audio ID. The 12D setting (V1 8D + V2 4D) offers the best quality–disentanglement trade-off.

4.4. Quantitative Evaluation

We evaluate reconstruction and cross-audio performance against recent state-of-the-art methods, including DiffDub [28], Diff2Lip [32], TalkLip [49], LatentSync [26], IP-LAP [64], and KeySync [2]. Results are shown in Tables 1 and 2, with full VBench metrics in Table C.4.

Both our FlashLips models achieve the best overall FID and FVD in both protocols, while also being substantially faster than the next-best method (up to $30.4\times$ vs. KeySync). On HyperIQA, we rank second and third with only marginal differences from the top model, a metric commonly used as a proxy for human perceptual quality, and obtain the highest VBench total score, indicating strong perceptual quality, temporal consistency, and background preservation.

In LipScore, our models are the top two in both protocols, ensuring highest lip-sync quality. In identity preservation (ID), we are first in reconstruction tied with LatentSync, and second in cross-audio behind it, tied with IP-LAP, while being up to $19.2\times$ and $25.8\times$ faster, respectively. This reflects strong lip–audio alignment and identity

retention across the full sequence.

For pixel-level metrics (PSNR, SSIM), we place third with a narrow gap, and second in LPIPS, showing that our one-step reconstruction maintains high image fidelity.

Overall, FlashLips delivers state-of-the-art visual and synchronization quality while maintaining faster-than-real-time throughput: **109.4 FPS** for the UNet and **66.8 FPS** for the Transformer base models. *User study results are provided in the supplementary materials.*

4.5. Qualitative Evaluation

Qualitative results in Fig. 5 and Fig. F.3 show that both FlashLips variants produce visually realistic, temporally coherent animations with strong identity preservation. Compared to existing approaches, our method yields smoother and more natural mouth motion without introducing artifacts or over-exaggerated animation. LatentSync and IP-LAP maintain identity reasonably well but often show weak lip–audio synchronization and noticeable visual artifacts; Diff2Lip exhibits similar issues. DiffDub and Wav2Lip exhibit identity drift and inconsistent lip motion, while KeySync struggles with large head poses, causing deformation and temporal instability. In contrast, FlashLips remains robust across more diverse viewing angles (Fig. F.4) and maintains stable lip–audio alignment. It also shows good generalization to out-of-distribution and non-human identities (Fig. F.5).

5. Ablation Study

Lips Encoder design and dimensionality. Our goal is a lips vector that (a) captures *configuration* of the lips and jaw and is easy to predict from audio, while (b) carrying minimal appearance information (skin tone, lip/teeth geometry) that should instead come from the reference identity latent. Lower appearance leakage simplifies Stage 2 (which cannot infer appearance from audio) and stabilizes training. It also improves pseudo-pair generation for self-refinement: with a well-disentangled vector, we can borrow lips-poses across identities to increase pose diversity.

We experiment with two principal variants. **(V1)** Use only the frozen expression encoder from [9] followed by a small projection head. **(V2)** Augment V1 with a small *residual* predicted from a lips crop (extracted via face parsing) by a lightweight ResNet. Table 5 shows that the **(V1)** variant already performs strongly with low identity leakage; reconstruction gains saturate around a lips vector of size 8. Adding a residual progressively improves reconstruction, but hurts disentanglement, especially after the residual reaches size 8. To test leakage, we substituted lips-pose vectors from different identities. We therefore adopt a **12D** mouth vector with an 8D encoder component + 4D residual, which offers a good trade-off: high reconstruction quality and low identity leakage.

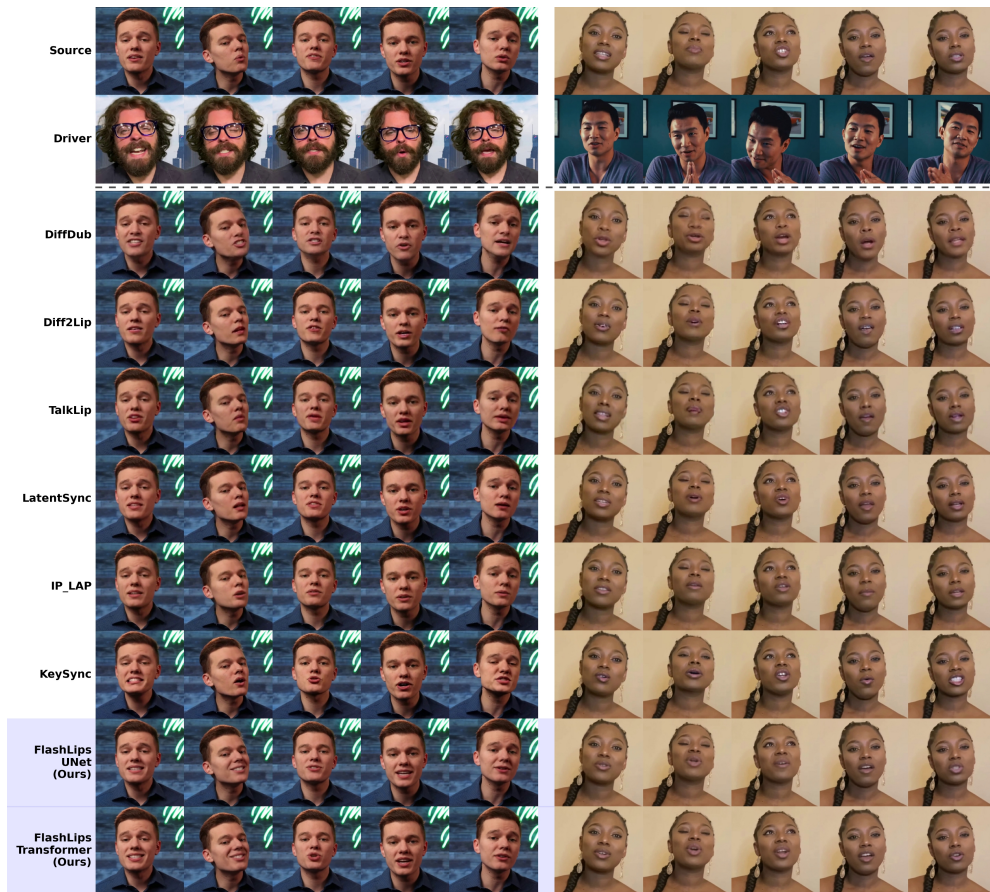


Figure 5. **Qualitative Comparison – Cross Audio.** Comparison with other lip-sync methods for cross-audio. The top two rows show the source and audio-driving videos, followed by lip-synced outputs from each method.

Number of reference frames. We vary the number of reference lips-pose vectors used in Stage 2. As shown in Tables 3 and 4, moving from 1 to 4 references improves identity preservation with negligible impact on sync; beyond 4 gains are marginal and we occasionally observe sync degradation—likely because too much identity information reduces the work done by audio-to-lips network and increases sensitivity when references come from a different clip at inference. We therefore use **4 reference frames**.

Stage 1 backbone: UNet vs. Transformer. Both backbones have similar accuracy (Table 1): the transformer is slightly better perceptually but slower, while the UNet is faster. We use the UNet for speed and the transformer for higher visual quality; architectural details are in the supplementary.

Summary. The ablations support three design choices used in the main results: a 12D lips-pose vector (8D encoder + 4D residual), four reference frames, and either a UNet (speed) or transformer (quality) backbone for Stage 1.

6. Conclusion

FlashLips shows that lip-sync can be posed as *deterministic editing*: a one-step, reconstruction-only latent editor driven by a flow-matched audio-to-lips module, with self-refinement removing the need of masks at inference. This yields a simple, modular system that runs faster than real time (>100 FPS with the UNet variant) while matching or surpassing recent diffusion/GAN baselines in visual quality, identity retention, and lip–audio alignment. Our analysis indicates that a compact, disentangled control vector plus self-refinement are sufficient to localize edits to the mouth, avoid identity/background drift, and decouple *what* to render from *how* to render, enabling practical dubbing and production use. Future work includes improving robustness under occlusions and extreme motion, and enriching the control space with prosody- and emotion-aware signals.

7. Acknowledgments

This work was conducted at Cantina Labs using their resources. We thank Ruslan Vorovchenko, Kacper Kania, and Jena Chelisev for their valuable assistance.

References

- [1] Alexei Baevski, Yuhao Zhou, Abdelrahman Mohamed, and Michael Auli. wav2vec 2.0: A framework for self-supervised learning of speech representations. *Advances in neural information processing systems*, 33:12449–12460, 2020. 2, 5
- [2] Antoni Bigata, Rodrigo Mira, Stella Bounareli, Michał Stypułkowski, Konstantinos Vougioukas, Stavros Petridis, and Maja Pantic. Keysync: A robust approach for leakage-free lip synchronization in high resolution, 2025. 2, 3, 6, 7
- [3] Antoni Bigata, Michał Stypułkowski, Rodrigo Mira, Stella Bounareli, Konstantinos Vougioukas, Zoe Landgraf, Nikita Drobyshev, Maciej Zieba, Stavros Petridis, and Maja Pantic. Keyface: Expressive audio-driven facial animation for long sequences via keyframe interpolation. In *Proceedings of the IEEE/CVF Conference on Computer Vision and Pattern Recognition (CVPR)*, pages 5477–5488, 2025. 3, 6
- [4] Dan Bigioi, Shubhajit Basak, Michał Stypułkowski, Maciej Zieba, Hugh Jordan, Rachel McDonnell, and Peter Corcoran. Speech driven video editing via an audio-conditioned diffusion model. *Image and Vision Computing*, 142:104911, 2024. 2, 3
- [5] Qiong Cao, Li Shen, Weidi Xie, Omkar M. Parkhi, and Andrew Zisserman. Vggface2: A dataset for recognising faces across pose and age, 2018. 4
- [6] Zhiyuan Chen, Jiajiong Cao, Zhiquan Chen, Yuming Li, and Chenguang Ma. Echomimic: Lifelike audio-driven portrait animations through editable landmark conditions. *Proceedings of the AAAI Conference on Artificial Intelligence*, 39: 2403–2410, 2025. 2
- [7] Joon Son Chung and Andrew Zisserman. Out of time: Automated lip sync in the wild. In *Computer Vision – ACCV 2016 Workshops*, pages 251–263, Cham, 2017. Springer International Publishing. 3
- [8] Jiahao Cui, Hui Li, Yun Zhan, Hanlin Shang, Kaihui Cheng, Yuqi Ma, Shan Mu, Hang Zhou, Jingdong Wang, and Siyu Zhu. Hallo3: Highly dynamic and realistic portrait image animation with video diffusion transformer, 2024. 5
- [9] Nikita Drobyshev, Antoni Bigata Casademunt, Konstantinos Vougioukas, Zoe Landgraf, Stavros Petridis, and Maja Pantic. Emoportraits: Emotion-enhanced multimodal one-shot head avatars, 2024. 4, 5, 7
- [10] Fangyu Du, Taiqing Li, Ziwei Zhang, Qian Qiao, Tan Yu, Dingcheng Zhen, Xu Jia, Yang Yang, Shunshun Yin, and Siyuan Liu. Rap: Real-time audio-driven portrait animation with video diffusion transformer, 2025. 2
- [11] Ian Goodfellow, Yoshua Bengio, Aaron Courville, and Yoshua Bengio. *Deep learning*. MIT Press, 2016. 2
- [12] Ian J Goodfellow, Jean Pouget-Abadie, Mehdi Mirza, Bing Xu, David Warde-Farley, Sherjil Ozair, Aaron Courville, and Yoshua Bengio. Generative adversarial nets. *Advances in neural information processing systems*, 27, 2014. 2
- [13] Jiazhi Guan, Zhanwang Zhang, Hang Zhou, Tianshu Hu, Kaisiyuan Wang, Dongliang He, Haocheng Feng, Jingtuo Liu, Errui Ding, Ziwei Liu, and Jingdong Wang. Stylesync: High-fidelity generalized and personalized lip sync in style-based generator. In *Proceedings of the IEEE/CVF Conference on Computer Vision and Pattern Recognition (CVPR)*, pages 1505–1515, 2023. 2, 3
- [14] Jiazhi Guan, Zhiliang Xu, Hang Zhou, Kaisiyuan Wang, Shengyi He, Zhanwang Zhang, Borong Liang, Haocheng Feng, Errui Ding, Jingtuo Liu, Jingdong Wang, Youjian Zhao, and Ziwei Liu. Resyncer: Rewiring style-based generator for unified audio-visually synced facial performer. In *Computer Vision – ECCV 2024*, pages 348–367, Cham, 2025. Springer Nature Switzerland. 3
- [15] Kaiming He, Xiangyu Zhang, Shaoqing Ren, and Jian Sun. Deep residual learning for image recognition. In *Proceedings of the IEEE Conference on Computer Vision and Pattern Recognition (CVPR)*, 2016. 4
- [16] Martin Heusel, Hubert Ramsauer, Thomas Unterthiner, Bernhard Nessler, and Sepp Hochreiter. Gans trained by a two time-scale update rule converge to a local nash equilibrium. In *Proceedings of the 31st International Conference on Neural Information Processing Systems*, page 6629–6640, Red Hook, NY, USA, 2017. Curran Associates Inc. 6
- [17] Ziqi Huang, Yanan He, Jiashuo Yu, Fan Zhang, Chenyang Si, Yuming Jiang, Yuanhan Zhang, Tianxing Wu, Qingyang Jin, Nattapol Chanpaisit, Yaohui Wang, Xinyuan Chen, Limin Wang, Dahua Lin, Yu Qiao, and Ziwei Liu. Vbench: Comprehensive benchmark suite for video generative models, 2023. 6, 3
- [18] Xiaozhong Ji, Xiaobin Hu, Zhihong Xu, Junwei Zhu, Chuming Lin, Qingdong He, Jiangning Zhang, Donghao Luo, Yi Chen, Qin Lin, Qinglin Lu, and Chengjie Wang. Sonic: Shifting focus to global audio perception in portrait animation. In *Proceedings of the IEEE/CVF Conference on Computer Vision and Pattern Recognition (CVPR)*, pages 193–203, 2025. 3
- [19] Jianwen Jiang, Chao Liang, Jiaqi Yang, Gaojie Lin, Tianyun Zhong, and Yanbo Zheng. Loopy: Taming audio-driven portrait avatar with long-term motion dependency, 2025. 3
- [20] Justin Johnson, Alexandre Alahi, and Li Fei-Fei. Perceptual losses for real-time style transfer and super-resolution. In *Computer Vision – ECCV 2016*, pages 694–711, Cham, 2016. Springer International Publishing. 4
- [21] Tero Karras, Samuli Laine, Miika Aittala, Janne Hellsten, Jaakko Lehtinen, and Timo Aila. Analyzing and improving the image quality of stylegan. In *Proceedings of the IEEE/CVF Conference on Computer Vision and Pattern Recognition (CVPR)*, 2020. 3
- [22] Taekyung Ki and Dongchan Min. Stylelipsync: Style-based personalized lip-sync video generation. In *Proceedings of the IEEE/CVF International Conference on Computer Vision (ICCV)*, pages 22841–22850, 2023. 3
- [23] Taekyung Ki, Dongchan Min, and Gyeongsu Chae. Float: Generative motion latent flow matching for audio-driven talking portrait. In *Proceedings of the IEEE/CVF International Conference on Computer Vision*, pages 14699–14710, 2025. 3
- [24] Diederik P. Kingma and Max Welling. Auto-Encoding Variational Bayes. In *2nd International Conference on Learning Representations, ICLR 2014, Banff, AB, Canada, April 14–16, 2014, Conference Track Proceedings*, 2014. 3

- [25] Tobias Kirschstein, Shenhan Qian, Simon Giebenhain, Tim Walter, and Matthias Nießner. Nersemble: Multi-view radiance field reconstruction of human heads. *ACM Transactions on Graphics (TOG)*, 42(4):1–14, 2023. 5
- [26] Chunyu Li, Chao Zhang, Weikai Xu, Jingyu Lin, Jinghui Xie, Weiguo Feng, Bingyue Peng, Cunjian Chen, and Weiwei Xing. Latentsync: Taming audio-conditioned latent diffusion models for lip sync with syncnet supervision, 2025. 2, 3, 6, 7
- [27] Yaron Lipman, Ricky TQ Chen, Heli Ben-Hamu, Maximilian Nickel, and Matt Le. Flow matching for generative modeling. *arXiv preprint arXiv:2210.02747*, 2022. 2, 5
- [28] Tao Liu, Chenpeng Du, Shuai Fan, Feilong Chen, and Kai Yu. Diffdub: Person-generic visual dubbing using inpainting renderer with diffusion auto-encoder. In *ICASSP 2024 - 2024 IEEE International Conference on Acoustics, Speech and Signal Processing (ICASSP)*, pages 3630–3634, 2024. 2, 3, 6, 7
- [29] Kingchao Liu, Chengyue Gong, and Qiang Liu. Flow straight and fast: Learning to generate and transfer data with rectified flow. *arXiv preprint arXiv:2209.03003*, 2022. 2, 5
- [30] Steven R Livingstone and Frank A Russo. The ryerson audio-visual database of emotional speech and song (ravdess): A dynamic, multimodal set of facial and vocal expressions in north american english. *PLoS one*, 13(5): e0196391, 2018. 5
- [31] Junxian Ma, Shiwen Wang, Jian Yang, Junyi Hu, Jian Liang, Guosheng Lin, Jingbo chen, Kai Li, and Yu Meng. Sayanything: Audio-driven lip synchronization with conditional video diffusion, 2025. 3
- [32] Soumik Mukhopadhyay, Saksham Suri, Ravi Teja Gadde, and Abhinav Shrivastava. Diff2lip: Audio conditioned diffusion models for lip-synchronization. In *Proceedings of the IEEE/CVF Winter Conference on Applications of Computer Vision (WACV)*, pages 5292–5302, 2024. 2, 3, 6, 7
- [33] Ziqiao Peng, Jiwen Liu, Haoxian Zhang, Xiaoqiang Liu, Songlin Tang, Pengfei Wan, Di Zhang, Hongyan Liu, and Jun He. Omnisync: Towards universal lip synchronization via diffusion transformers, 2025. 2, 3
- [34] Dustin Podell, Zion English, Kyle Lacey, Andreas Blattmann, Tim Dockhorn, Jonas Müller, Joe Penna, and Robin Rombach. Sdxl: Improving latent diffusion models for high-resolution image synthesis, 2023. 2, 3
- [35] KR Prajwal, Vinay P Nambodiri, C Aguerrebere, C Theobalt, L Jeni, and Rudrabha T G. A lip-sync expert is all you need for speech to lip generation in the wild. In *Proceedings of the 28th ACM International Conference on Multimedia*, pages 484–492, 2020. 2, 3
- [36] Robin Rombach, Andreas Blattmann, Dominik Lorenz, Patrick Esser, and Bjorn Ommer. High-resolution image synthesis with latent diffusion models. In *Proceedings of the IEEE/CVF conference on computer vision and pattern recognition*, pages 10674–10685, 2022. 3
- [37] Tim Salimans, Ian Goodfellow, Wojciech Zaremba, Vicki Cheung, Alec Radford, Xi Chen, and Xi Chen. Improved techniques for training gans. In *Advances in Neural Information Processing Systems*. Curran Associates, Inc., 2016. 2
- [38] Florian Schroff, Dmitry Kalenichenko, and James Philbin. Facenet: A unified embedding for face recognition and clustering. In *2015 IEEE Conference on Computer Vision and Pattern Recognition (CVPR)*, page 815–823. IEEE, 2015. 6
- [39] Sefik Serengil and Alper Ozpinar. A benchmark of facial recognition pipelines and co-usability performances of modules. *Journal of Information Technologies*, 17(2):95–107, 2024. 6
- [40] Jiamāo Shen, Yidi Zhou, Zhiyao Liu, Jing Wang, and Jian Wang. Diftalk: A diffusion model for realistic talking head generation. In *Thirty-seventh Conference on Neural Information Processing Systems*, 2023. 2
- [41] Akash Srivastava, Lazar Valkov, Chris Russell, Michael U. Gutmann, and Charles Sutton. Veegan: Reducing mode collapse in gans using implicit variational learning. In *Advances in Neural Information Processing Systems*. Curran Associates, Inc., 2017. 2
- [42] Michał Stypułkowski, Konstantinos Vougioukas, Sen He, Maciej Zieba, Stavros Petridis, and Maja Pantic. Diffused heads: Diffusion models beat gans on talking-face generation. In *Proceedings of the IEEE/CVF Winter Conference on Applications of Computer Vision (WACV)*, pages 5091–5100, 2024. 2, 3
- [43] Shaolin Su, Qingsen Yan, Yu Zhu, Cheng Zhang, Xin Ge, Jinqiu Sun, and Yanning Zhang. Blindly assess image quality in the wild guided by a self-adaptive hyper network. In *Proceedings of the IEEE/CVF Conference on Computer Vision and Pattern Recognition (CVPR)*, 2020. 6
- [44] Linrui Tian, Qi Wang, Bang Zhang, and Liefeng Bo. Emo: Emote portrait alive generating expressive portrait videos with audio2video diffusion model under weak conditions. In *Computer Vision – ECCV 2024*, pages 244–260, Cham, 2025. Springer Nature Switzerland. 3
- [45] Thomas Unterthiner, Sjoerd van Steenkiste, Karol Kurach, Raphael Marinier, Marcin Michalski, and Sylvain Gelly. Towards accurate generative models of video: A new metric & challenges, 2019. 6
- [46] Konstantinos Vougioukas, Stavros Petridis, and Maja Pantic. End-to-end speech-driven facial animation with temporal gans. In *British Machine Vision Conference*, 2018. 3
- [47] Konstantinos Vougioukas, Stavros Petridis, and Maja Pantic. Realistic speech-driven facial animation with gans. *International Journal of Computer Vision*, 128, 2020. 2, 3
- [48] Cong Wang, Kuan Tian, Jun Zhang, Yonghang Guan, Feng Luo, Fei Shen, Zhiwei Jiang, Qing Gu, Xiao Han, and Wei Yang. V-express: Conditional dropout for progressive training of portrait video generation, 2024. 2
- [49] Jiadong Wang, Xinyuan Qian, Malu Zhang, Robby T Tan, and Haizhou Li. Seeing what you said: Talking face generation guided by a lip reading expert. In *Proceedings of the IEEE/CVF Conference on Computer Vision and Pattern Recognition*, pages 14653–14662, 2023. 3, 6, 7
- [50] Kaisiyuan Wang, Qianyi Wu, Linsen Song, Zhuoqian Yang, Wayne Wu, Chen Qian, Ran He, Yu Qiao, and Chen Change Loy. Mead: A large-scale audio-visual dataset for emotional talking-face generation. In *ECCV*, 2020. 5
- [51] Zhou Wang, A.C. Bovik, H.R. Sheikh, and E.P. Simoncelli. Image quality assessment: from error visibility to structural

- similarity. *IEEE Transactions on Image Processing*, 13(4): 600–612, 2004. 6
- [52] Huawei Wei, Zejun Yang, and Zhisheng Wang. Aniportrait: Audio-driven synthesis of photorealistic portrait animation, 2024. 3
- [53] Mingwang Xu, Hui Li, Qingkun Su, Hanlin Shang, Liwei Zhang, Ce Liu, Jingdong Wang, Yao Yao, and Siyu Zhu. Hallo: Hierarchical audio-driven visual synthesis for portrait image animation, 2024. 2, 3
- [54] Sicheng Xu, Guojun Chen, Yu-Xiao Guo, Jiaolong Yang, Chong Li, Zhenyu Zang, Yizhong Zhang, Xin Tong, and Baining Guo. Vasa-1: Lifelike audio-driven talking faces generated in real time. *Advances in Neural Information Processing Systems*, 37:660–684, 2024. 3
- [55] Jianhui Yu, Hao Zhu, Liming Jiang, Chen Change Loy, Weidong Cai, and Wayne Wu. CelebV-Text: A large-scale facial text-video dataset. In *CVPR*, 2023. 5
- [56] Chenxu Zhang, Chao Wang, Jianfeng Zhang, Hongyi Xu, Guoxian Song, You Xie, Linjie Luo, Yapeng Tian, Xiaohu Guo, and Jiashi Feng. Dream-talk: Diffusion-based realistic emotional audio-driven method for single image talking face generation, 2023. 3
- [57] Richard Zhang, Phillip Isola, Alexei A Efros, Eli Shechtman, and Oliver Wang. The unreasonable effectiveness of deep features as a perceptual metric. In *CVPR*, 2018. 6
- [58] Wenxuan Zhang, Xiaodong Cun, Xuan Wang, Yong Zhang, Xi Shen, Yu Guo, Ying Shan, and Fei Wang. Sadtalker: Learning realistic 3d motion coefficients for stylized audio-driven single image talking face animation. In *Proceedings of the IEEE/CVF Conference on Computer Vision and Pattern Recognition (CVPR)*, pages 8652–8661, 2023. 3
- [59] Yifeng Zhang, Zhipeng Liu, Jin Yan, and Chun Li. Dreamtalk: When expressive 3d talking head generation meets diffusion probabilistic models. In *Proceedings of the AAAI Conference on Artificial Intelligence*, pages 5555–5563, 2024. 2
- [60] Yue Zhang, Zhizhou Zhong, Minhao Liu, Zhaokang Chen, Bin Wu, Yubin Zeng, Chao Zhan, Yingjie He, Junxin Huang, and Wenjiang Zhou. Musetalk: Real-time high-fidelity video dubbing via spatio-temporal sampling, 2025. 3
- [61] Zhimeng Zhang, Lincheng Li, Yu Ding, and Changjie Fan. Flow-guided one-shot talking face generation with a high-resolution audio-visual dataset. In *Proceedings of the IEEE/CVF Conference on Computer Vision and Pattern Recognition*, pages 3661–3670, 2021. 5
- [62] Zhimeng Zhang, Zhipeng Hu, Wenjin Deng, Changjie Fan, Tangjie Lv, and Yu Ding. Dinet: Deformation inpainting network for realistic face visually dubbing on high resolution video. In *AAAI Conference on Artificial Intelligence*, 2023. 2, 3
- [63] Rui Zhen, Wenchao Song, Qiang He, Juan Cao, Lei Shi, and Jia Luo. Human-computer interaction system: A survey of talking-head generation. *Electronics*, 12(1), 2023. 2
- [64] Weizhi Zhong, Chaowei Fang, Yinqi Cai, Pengxu Wei, Gangming Zhao, Liang Lin, and Guanbin Li. Identity-preserving talking face generation with landmark and appearance priors. In *Proceedings of the IEEE/CVF Conference on Computer Vision and Pattern Recognition (CVPR)*, pages 9729–9738, 2023. 3, 6, 7
- [65] Hang Zhou, Yu Liu, Ziwei Liu, Ping Luo, and Xiaogang Wang. Talking face generation by adversarially disentangled audio-visual representation. In *Proceedings of the AAAI conference on artificial intelligence*, pages 9299–9306, 2019. 2, 3
- [66] Hang Zhou, Yasheng Sun, Wayne Wu, Chen Change Loy, Xiaogang Wang, and Ziwei Liu. Pose-controllable talking face generation by implicitly modularized audio-visual representation. In *Proceedings of the IEEE/CVF Conference on Computer Vision and Pattern Recognition (CVPR)*, pages 4176–4186, 2021. 3
- [67] Hao Zhu, Wayne Wu, Wentao Zhu, Liming Jiang, Siwei Tang, Li Zhang, Ziwei Liu, and Chen Change Loy. CelebV-HQ: A large-scale video facial attributes dataset. In *ECCV*, 2022. 5

FlashLips: 100-FPS Mask-Free Latent Lip-Sync using Reconstruction Instead of Diffusion or GANs

Supplementary Material

A. Training Details

A.1. Data Augmentation

During training for both stages, we apply the following augmentations. All images are normalized by dividing by 255 to map pixel values into the range $[0, 1]$. For Stage 1, we additionally apply random horizontal flips with probability 0.5 and ColorJitter with a coefficient of 0.4 for hue, brightness, and contrast, 3.2 for saturation, and an overall application probability of 0.9. For the distilled mouth-latent network, we downscale the source image to 384×384 using interpolation.

A.2. Mask Removal Training Details

After the reconstruction editor R_ϕ converges, we synthesize lip-altered counterparts for real frames. Given a real frame S and a sampled lips-pose vector \mathbf{z}_{lips} , we produce $\tilde{S} = R_\phi(S; \mathbf{z}_{\text{lips}})$ and form symmetric pseudo-pairs ($S \rightarrow \tilde{S}$) and ($\tilde{S} \rightarrow S$). We initialize the *LipsChange* editor $L_\theta \leftarrow R_\phi$ and fine-tune it on these pairs using the same objective as in Section 3.1.3. At test time, L_θ runs *without* any explicit mouth masks.

Why two directions?

- ($S \rightarrow \tilde{S}$) (**real** \rightarrow **synth**): input matches inference (real frames), which preserves lip-audio sync; however, the target \tilde{S} may contain minor artifacts from R_ϕ , so training *only* on this direction can reproduce them.
- ($\tilde{S} \rightarrow S$) (**synth** \rightarrow **real**): target is clean (real S), which discourages artifacts; but the input is synthetic and does not match inference, so training *only* on this direction hurts sync/generalization.

Mixture. We tried various training strategies, but eventually we train our model on a mixture of both directions: sample ($S \rightarrow \tilde{S}$) with probability 2/3 and ($\tilde{S} \rightarrow S$) with probability 1/3. Empirically, this preserves lip-audio alignment (same LipScore as the real \rightarrow synth-only variant) while improving visual quality by avoiding propagation of reconstruction artifacts. This self-refinement removes the need for external segmentation at inference and keeps the pipeline mask-free.

A.3. Architecture Details

All Stage 1 editors (Reconstruction and *LipsChange*) operate on the SDXL VAE latent grid (stride 8). The *input*

is the channel-wise concatenation of the masked target latent, the identity-adapted reference latent $f_{\text{ref}}(\mathbf{z}_{\text{ref}})$, and the lips-pose vector tiled to the latent resolution; this totals **52** channels in our implementation. The network predicts a **4-channel latent residual** that is added to the masked latent and decoded by the frozen VAE. *LipsChange* shares the same backbone and is initialized from the Reconstruction network weights for mask-free self-refinement.

UNet. Table A.1 summarizes the UNet model: we use ResNet2D blocks (GroupNorm (GN) 32, SiLU, 3×3 convolutions). The down path increases the number of channels from $384 \rightarrow 512 \rightarrow 640$ using average-pooling for downsampling; the up path mirrors this structure with skip concatenations and resize-conv upsampling, ending with GN+SiLU+Conv to 4 channels. This backbone yields the best throughput (see Table 2) while preserving identity and background consistency and confining edits to the mouth.

Stage	Composition	Channels (in \rightarrow out)
Input	Conv2d($k=3, s=1, p=1$)	52 \rightarrow 384
Down Block 1	$4 \times$ ResNet2D + $1 \times$ ResNet2D (with AvgPool Downsample)	384 \rightarrow 384
Down Block 2	$4 \times$ ResNet2D + $1 \times$ ResNet2D (with AvgPool Downsample)	384 \rightarrow 512
Down Block 3	$4 \times$ ResNet2D (no downsampling)	512 \rightarrow 640
Mid Block	$2 \times$ ResNet2D	640 \rightarrow 640
Up Block 1	$5 \times$ ResNet2D + $1 \times$ ResNet2D (with Upsample)	1280 \rightarrow 640
Up Block 2	$5 \times$ ResNet2D + $1 \times$ ResNet2D (with Upsample)	1152 \rightarrow 512
Up Block 3	$5 \times$ ResNet2D (no upsampling)	896 \rightarrow 384
Output	GN(32) + SiLU + Conv2d($k=3, s=1, p=1$)	384 \rightarrow 4

Table A.1. **Architecture of the UNet Base Model.** Each ResNet2D block consists of GroupNorm (GN, 32 groups), SiLU activation, and two Conv2d layers ($k=3, s=1, p=1$).

Transformer. Table A.2 summarizes the ViT-style model: a 1×1 input projection ($52 \rightarrow 128$), followed by GN and a 1×1 lift to 1024 channels; then 16 BasicTransformerBlocks (LayerNorm, MHSA with 16 heads \times 64 dim, GEGLU MLP with $4 \times$ expansion); followed by 1×1 projections back to 4 output channels. Convolutional pre-/post-projections preserve the 2D grid, while attention improves global consistency at the cost of lower FPS.

Stage	Composition	Channels (in \rightarrow out)
Input Projection	Conv2d($k=1, s=1$)	52 \rightarrow 128
Transformer Pre-projection	GroupNorm(32) + Conv2d($k=1, s=1$)	128 \rightarrow 1024
Transformer Blocks	$16 \times$ BasicTransformerBlock: LayerNorm + MHSA (16 heads, 64-dim/head) + LayerNorm + FeedForward (GEGLU, $4 \times$ expansion)	1024 \rightarrow 1024
Transformer Post-projection	Conv2d($k=1, s=1$)	1024 \rightarrow 128
Output Projection	Conv2d($k=1, s=1$)	128 \rightarrow 4

Table A.2. **Architecture of the Transformer Base Model.** MHSA stands for Multi-Head Self-Attention.

Trade-off. Both backbones achieve comparable accuracy (main paper). The transformer is slightly stronger on perceptual metrics, whereas the UNet is substantially faster. This makes the UNet preferable for real-time use and the transformer preferable for peak visual quality. The Stage-2 flow-matching transformer (FMT) architecture – shared by both UNet and Transformer variants of FlashLips – is detailed in Table A.3.

Stage	Composition	Dims (in → out)
Input Motion Embedding	SequenceEmbed: Linear($d_w + d_p \rightarrow d_h$) (no affine norm)	$(d_w + d_p) \rightarrow d_h$ (12+16) → 1024
Positional Encoding	Fixed sinusoidal encoding (non-learnable), added to token embeddings ($T = 60$ frames)	$T \times d_h \rightarrow T \times d_h$ $60 \times 1024 \rightarrow 60 \times 1024$
Time Embedding	TimestepEmbedder: sinusoidal (256-dim) + MLP: Linear(256 → d_h) + SiLU + Linear($d_h \rightarrow d_h$)	$256 \rightarrow d_h$ $256 \rightarrow 1024$ $1024 \rightarrow 1024$
Condition Embedding	Concat of identity, audio and emotion latents: [w_r, w_a, w_e] with Linear($d_{\text{cond}} \rightarrow d_h$)	$(d_{\text{cond}} \rightarrow d_h)$ $d_{\text{cond}} = d_w \cdot n_{\text{id}} + d_a + d_e$ ($12n_{\text{id}} + 512 + 7$) → 1024
FMT Blocks	8 × FMTBlock: AdaLN-modulated MHSA (8 heads, 128-dim/head) + AdaLN-modulated MLP MLP: Linear($d_h \rightarrow 4d_h$) + GELU + Linear($4d_h \rightarrow d_h$) AdaLN MLP: SiLU + Linear($d_h \rightarrow 6d_h$)	$d_h \rightarrow d_h$ $1024 \rightarrow 1024$ $1024 \rightarrow 4096$ $4096 \rightarrow 1024$ $1024 \rightarrow 6144$
Output Decoder	AdaLN: LayerNorm (no affine) + SiLU + Linear($d_h \rightarrow 2d_h$) Linear($d_h \rightarrow d_w$)	$d_h \rightarrow d_h$ $1024 \rightarrow 2048$ $1024 \rightarrow 12$

Table A.3. **Architecture of the Flow Matching Transformer (FMT).** d_w is the motion latent dimension, d_p is the pose latent dimension, d_h is the hidden size. MHSA stands for Multi-Head Self-Attention.

B. User Study

To complement our quantitative evaluation, we conducted a user study comparing FlashLips with several baseline lip-sync models. Using the same 100 cross-audio videos as in our quantitative experiments, we present participants with two videos per trial: one generated by our method and one by a randomly selected baseline. Users evaluate either *Visual Quality* or *Lip Sync*, choosing the preferred video or indicating that both are of the same quality. We collect up to 700 votes per baseline comparison and setting, which are then aggregated. The results are shown in Figure C.1.

Across nearly all baselines, FlashLips is the clear user preference for both visual quality and lip-sync accuracy, with a substantial portion of responses also indicating comparable quality. We outperform DiffDub, Diff2Lip, TalkLip, and IP_LAP by a large margin, with only a minority of votes favoring the competing models. Against LatentSync, most users judge the outputs to be similar, with a slight preference for our method. KeySync – a considerably slower (by $\times 30.4$ times, see Table 2) iterative diffusion model – shows a negligible advantage with 29.0% vs 32.7% of votes for visual quality and 26.6% vs 28.4% for lip-sync, although the vast majority of users still deem the two videos to be of equal quality with 38.3% and 45.0% of votes in the respective settings. We attribute this small disadvantage to

artifacts introduced by the SDXL VAE under certain framings and head poses (see Section D).

Overall, the study highlights that FlashLips delivers competitive or superior perceptual quality while operating orders of magnitude faster than state-of-the-art diffusion-based approaches.

C. Additional Quantitative Results

C.1. Mask Removal: Quantitative Impact

To isolate the effect of removing explicit mouth masks, Table C.5 compares the *Transformer with Mask* to our mask-free editors *Transformer Mask-free* and *UNet Mask-free* under identical evaluation protocols. We treat reconstruction as a sanity check and focus primarily on cross-audio, which reflects the real use case of our model.

Reconstruction. Removing the mask improves both fidelity and lip-sync quality for the Transformer variant: LipScore increases from roughly 0.50 to 0.70–0.75, and all fidelity metrics (FID/FVD, LPIPS, PSNR, SSIM, ID) move in the expected direction, suggesting better distribution match, sharper frames and higher identity similarity. This confirms that mask-free editing can localize mouth modifications without sacrificing reconstruction quality.

Cross-audio. Mask removal yields the largest improvements in cross-audio. For the Transformer, FID drops from ~ 10.2 to ~ 5.7 and FVD from ~ 74 to ~ 25 –41, indicating cleaner frames and substantially more stable motion. ID improves from ~ 0.77 –0.79 to ~ 0.81 –0.82, and HyperIQA increases slightly. LipScore remains in the same range of 0.35–0.40, showing that lip–audio alignment is preserved. Qualitatively, mask-free models reduce mouth glitches and flicker while providing more stable backgrounds and facial detail. The mask-free UNet follows the same trend, with slightly worse FID/FVD but higher throughput.

Takeaway. Mask-free self-refinement is a key contributor to the final system: it removes the need for segmentation at inference and consistently improves perceptual quality, temporal smoothness, and identity preservation, while maintaining lip–audio alignment comparable to or better than the masked baseline.

C.2. VBench Results

Table C.4 summarizes VBench scores (see Section 4.3). Across both reconstruction and cross-audio settings, our mask-free models achieve the highest or near-highest total score, demonstrating strong subject and background consistency, motion smoothness, and perceived visual fidelity.

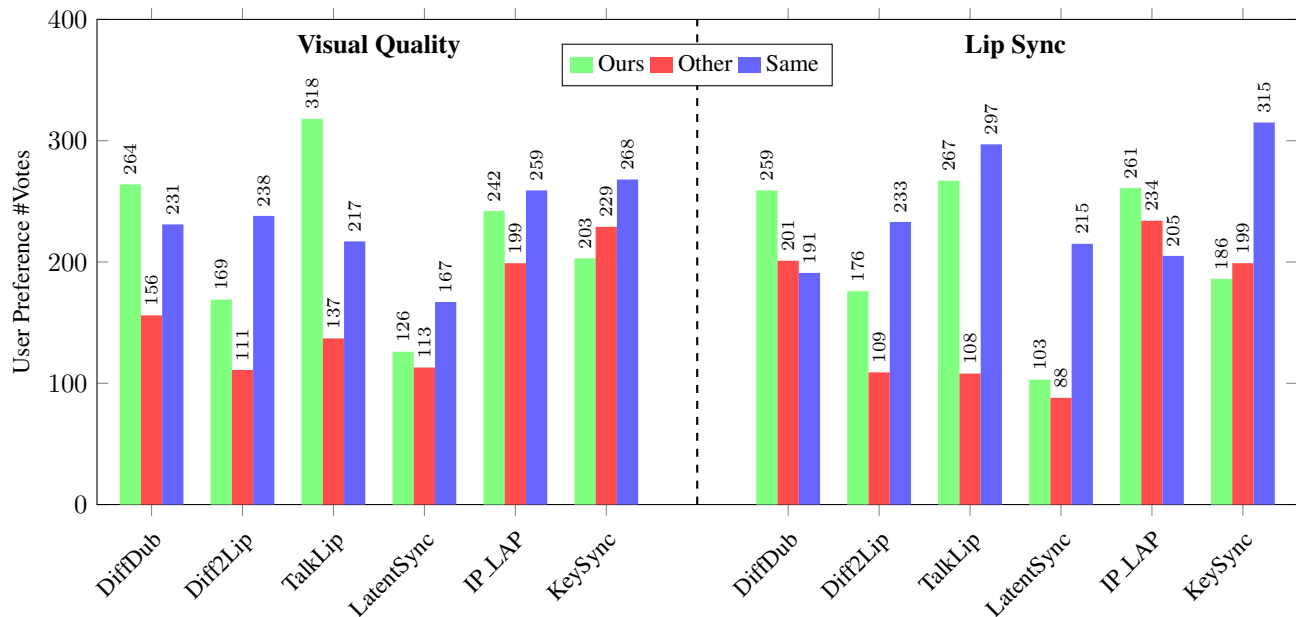


Figure C.1. **Human Preference Evaluation.** We conducted a user study comparing FlashLips against randomly selected baseline models. Participants indicated their preference across two criteria: Visual Quality and Lip Sync. The chart displays the number of responses favoring our model (Ours), the competing model (Other), or neither (Same).

Model	Reconstruction						
	SC \uparrow	BC \uparrow	MS \uparrow	DD \uparrow	AQ \uparrow	IQ \uparrow	Total \uparrow
DiffDub [28]	0.962	0.954	0.992	0.670	0.505	0.661	0.673
Diff2Lip [32]	0.953	0.946	0.992	0.653	0.557	0.633	0.672
TalkLip [49]	0.952	0.942	0.992	<u>0.727</u>	0.528	0.596	0.667
LatentSync [26]	0.967	0.948	<u>0.991</u>	0.723	0.528	0.671	<u>0.682</u>
IP_LAP [64]	0.961	0.945	0.992	0.720	0.519	0.640	0.674
KeySync [2]	0.953	0.948	<u>0.991</u>	0.750	0.531	<u>0.669</u>	0.681
FlashLips – UNet (Ours)	0.957	0.956	0.990	0.750	<u>0.559</u>	0.667	0.687
FlashLips – Transformer (Ours)	0.957	<u>0.955</u>	0.990	0.750	0.560	<u>0.669</u>	0.687

Model	Cross-Audio						
	SC \uparrow	BC \uparrow	MS \uparrow	DD \uparrow	AQ \uparrow	IQ \uparrow	Total \uparrow
DiffDub [28]	0.956	0.953	0.992	0.624	0.506	0.660	0.668
Diff2Lip [32]	0.946	0.945	<u>0.991</u>	0.622	0.550	0.631	0.667
TalkLip [49]	<u>0.958</u>	0.947	0.992	0.420	0.527	0.596	0.645
LatentSync [26]	0.963	0.953	<u>0.991</u>	0.690	0.537	0.664	0.680
IP_LAP [64]	0.963	0.945	0.992	0.670	0.519	0.639	0.670
KeySync [2]	0.951	0.949	<u>0.991</u>	<u>0.680</u>	0.529	0.668	0.676
FlashLips – UNet (Ours)	0.955	0.958	0.990	0.670	<u>0.558</u>	<u>0.666</u>	<u>0.681</u>
FlashLips – Transformer (Ours)	0.955	<u>0.957</u>	0.990	<u>0.680</u>	0.559	0.668	0.682

Table C.4. **Quantitative Comparison on VBench.** Video quality evaluation using VBench [17] metrics on 100 randomly sampled reconstruction videos and 100 cross-audio pairs from HDTF, CelebV-HQ and CelebV-Text. Metrics defined in Section 4.3.

D. Limitations

Although our model produces high-quality lip-sync in most cases, it still exhibits some limitations (Figure C.2). Since the method relies on direct prediction rather than the iterative denoising used in diffusion-based approaches, it can struggle to generate fine-grained facial details, particularly



Figure C.2. **Limitations.** Examples illustrating typical failure cases under challenging conditions, including generating facial hair and teeth details, occlusions, and artifacts caused by the SDXL VAE.

in regions such as facial hair and teeth. While the model was not explicitly trained to handle occlusions, it is often surprisingly robust; however, occluding objects can still degrade lip-sync accuracy in more challenging sequences. A more fundamental limitation stems from the SDXL VAE, whose performance degrades in a predictable manner under certain framings and head poses. The VAE performs well on tight close-ups, but when the subject appears in wider shots, artifacts become more common and can adversely affect the lip-sync quality.

Model	# Ref Lats	FID ↓	FVD ↓	HyperIQA ↑	LipScore ↑	ID ↑	PSNR ↑	SSIM ↑	LPIPS ↓
Reconstruction									
Transformer with Mask	1	8.06	57.80	73.26	0.50	0.81	27.68	0.90	0.044
	4	8.01	57.93	73.27	0.53	0.82	27.75	0.90	0.043
	8	7.95	58.15	73.28	0.55	0.82	27.77	0.90	0.043
	16	7.97	57.78	73.29	0.56	0.82	27.79	0.90	0.043
	32	7.94	57.63	73.28	0.55	0.82	27.80	0.90	0.043
Transformer Mask-free	1	4.46	12.53	74.05	0.69	0.85	32.71	0.94	0.021
	4	4.43	12.31	74.06	0.71	0.86	32.88	0.94	0.021
	8	4.41	12.47	74.07	0.73	0.85	33.00	0.94	0.021
	16	4.38	11.90	74.08	0.74	0.86	33.02	0.94	0.021
	32	4.36	12.16	74.08	0.75	0.86	33.10	0.94	0.020
UNet Mask-free	1	4.73	15.68	73.79	0.67	0.85	32.74	0.94	0.022
	4	4.75	15.20	73.81	0.70	0.85	32.86	0.94	0.022
	8	4.76	15.61	73.82	0.70	0.85	32.92	0.94	0.022
	16	4.66	15.07	73.83	0.71	0.85	32.95	0.94	0.022
	32	4.70	15.85	73.83	0.69	0.85	32.97	0.94	0.022
Cross-Audio									
Transformer with Mask	1	10.24	73.91	73.16	0.40	0.77	–	–	–
	4	9.87	68.10	73.23	0.39	0.77	–	–	–
	8	9.74	68.77	73.26	0.38	0.78	–	–	–
	16	9.67	66.17	73.25	0.35	0.79	–	–	–
	32	9.68	64.92	73.25	0.34	0.78	–	–	–
Transformer Mask-free	1	6.25	41.38	73.80	0.40	0.79	–	–	–
	4	5.89	29.40	73.84	0.37	0.81	–	–	–
	8	5.81	29.54	73.88	0.35	0.81	–	–	–
	16	5.73	26.35	73.88	0.34	0.81	–	–	–
	32	5.68	25.16	73.89	0.32	0.82	–	–	–
UNet Mask-free	1	6.54	42.78	73.51	0.40	0.79	–	–	–
	4	6.23	33.57	73.58	0.38	0.81	–	–	–
	8	6.13	32.64	73.61	0.36	0.80	–	–	–
	16	6.07	31.34	73.63	0.34	0.81	–	–	–
	32	6.13	28.54	73.63	0.32	0.81	–	–	–

Table C.5. **Full Ablation Study.** Ablation study of our mask and mask-free models, and different numbers of references for the audio-to-latent model for reconstruction and cross-audio. Metrics computed on 100 randomly sampled reconstruction videos and 100 cross-audio pairs from HDTF, CelebV-HQ and CelebV-Text.

E. Ethical Considerations and Societal Impact

Lip-sync technology enables applications such as accessibility tools, film and TV dubbing, translation for non-native audiences, expressive avatars, and content creation. It also carries clear risks: malicious users may create deceptive deepfakes, spread misinformation, or impersonate identities. Our method is intended for beneficial use, and we explicitly discourage any harmful or non-consensual deployment. Any system that alters a person’s likeness should obtain explicit, informed consent.

Our model is trained on publicly available datasets that follow their usage guidelines and on an internal dataset collected with participant consent. As with many audio-

visual models, dataset limitations may bring biases across attributes as skin tone, facial structure, language, or accent.

F. Additional Qualitative Results

We provide qualitative reconstruction results in Figure F.3, comparing FlashLips against all baselines. We also assess visual quality across diverse source–driver head-pose combinations, including frontal–frontal, side–side, side–frontal, and frontal–side pairs (Figure F.4). Finally, we show results on out-of-distribution subjects – synthetic human faces and non-human or stylized characters – to demonstrate that our method remains robust and generalizable under these more challenging conditions (Figure F.5).



Figure F.3. **Qualitative Comparison – Reconstruction.** Comparisons with other lip-sync methods for reconstruction. The first row shows the source video; the following rows display the inferred lip-synced videos by each method.

Frontal to Frontal



Side to Side



Side to Frontal



Frontal to Side



Figure F.4. Lip-sync results across varying facial pose combinations. Each triplet shows a source video, video corresponding to the audio driver, and the resulting prediction.



Figure F.5. **Lip-sync results on out-of-distribution (OOD) faces.** The top block of images shows results on generated human faces, while the lower block shows results on non-human or stylized faces. Our method maintains consistent lip synchronization and natural articulation across both domains.